Colloids and Surfaces B: Biointerfaces 217 (2022) 112636

Contents lists available at ScienceDirect

Colloids and Surfaces B: Biointerfaces

journal homepage: www.elsevier.com/locate/colsurfb

Interactions between curcumin and cell membrane models by Langmuir monolayers

María Pedrosa [a,b], Julia Maldonado-Valderrama [a,b], María José Gálvez-Ruiz [a,b,*]

[a] Biocolloids and Fluid Physics Group, Department of Applied Physics, University of Granada, Campus Fuente Nueva, s/n, C.P. 18071, Granada, Spain
[b] Excellence Research Unit "Modeling Nature" (MNat), University of Granada, Cuesta del Hospicio, s/n, C.P. 18010, Granada, Spain

ARTICLE INFO

Keywords:
Cell membrane model
Curcumin
Langmuir monolayers
Compressibility
Brewster Angle Microscopy
Atomic Force Microscopy

ABSTRACT

Studying interactions between potential anticancer drugs and cell membrane models is of great interest to explore the capability of novel drugs in the development of anticancer treatments. Lipid membrane models are useful to understand cellular interactions and to discern drug mechanism action. Here, the interactions of curcumin, as a bioactive natural compound with anti-cancer properties, with both healthy and cancerous or tumor cell membrane models, based on Langmuir monolayers, have been studied. The healthy-cell membrane model is composed of cholesterol 67%, and saturated lipid dipalmitoylphosphatidylcholine 33%. The cancerous-cell-membrane-model is composed of a lower proportion of cholesterol, 25%, and unsaturated lipid sphingomyelin 75%. To compare their interaction with curcumin we report the compression isotherms registered for both lipid membrane models and curcumin in different proportions, their compression moduli and the thermodynamic interaction parameters. From this analysis, we evidence a destabilizing interaction between curcumin and the cancerous cell membrane model in comparison with the healthy one. This interaction is further visualized by micro-Brewster Angle and Atomic Force Microscopies. Our experiments show that the drug enhances cohesion in the healthy membrane model whereas it fluidifies the cancerous cell membrane model causing thermodynamic destabilization. These are useful results to improve the selectivity of the drug avoiding adverse side effects of most current anticancer therapies.

1. Introduction

The rational design of novel drugs or effective nanosystems loaded with drugs and/or bioactive molecules requires previous and complex knowledge of the interaction of drugs or nanosystems with biological media. Of particular interest is the target identification by the drug or bioactive molecule. In the case of the development of anti-cancer drugs or drug nanocarriers, their ability to identify the cancerous cell peculiarities and the markers or tumor receptors is highly relevant. In this sense, it is well known that the lipid composition of the cancerous cell membranes differs from the healthy cell membranes [1–4]. Further, the lipid membrane is the mean barrier that the drug or nanocarrier must overcome to introduce the drug into the cell. All these considerations are fundamental to elucidate the action mechanism of the drug and to improve the therapeutic strategies. In this paper, we focus our attention on the interaction between a bioactive natural compound with anti-cancer properties – curcumin (Cur) - and cell membrane models.

Due to the additional difficulties to isolate and manipulate real cell membranes, many different cell membrane models, such as supported lipid bilayer, vesicle, liposome, and lipid monolayer, have been used in research in the past [5,6]. Langmuir monolayers at the air-water interface have been widely used to mimic cell membranes in attempts to determine the mechanisms involved in their interaction with bioactive molecules as this technique allows fine control over the composition and packing of the membrane model [3]. Popular compounds used to prepare Langmuir monolayers are lipids, as their monolayers are considered as a model for half a cell membrane [7–10].

Replicating the composition of a model membrane is also an arduous

Abbreviations: DPPC, dipalmitoylphosphatidylcholine; Cur, curcumin; Chol, cholesterol; Sph, sphingomyelin; DMPC, 1,2-dimyristoyl-sn-glycero-3-phosphochloline; DMPS, 1,2-dimyristoyl-sn-glycero-3phospho-L-serine; DHP, dihexadecyl phosphate; DPPG, dipalmitoylphosphatidylglycerol; EYPC, egg yolk phosphatidylcholine; AFM, Atomic Force Microscopy, MicroBAM, micro-Brewster Angle Microscopy.

* Corresponding author at: Biocolloids and Fluid Physics Group, Department of Applied Physics, University of Granada, Campus Fuente Nueva, s/n, C.P. 18071, Granada, Spain.

E-mail address: mjgalvez@ugr.es (M.J. Gálvez-Ruiz).

https://doi.org/10.1016/j.colsurfb.2022.112636
Received 27 March 2022; Received in revised form 9 June 2022; Accepted 11 June 2022
Available online 17 June 2022

task since the lipid composition varies greatly on cell type. Moreover, for the same type of cell, the ratio of the component lipids of membranes is different for both healthy and cancer cells and also, it depends on the degree of malignancy. Accordingly, there is an enormous variety of different correlations between membranes of healthy and tumor cells [11]. For instance, van Blitterswijk et al. evidenced that the membrane of leukemic murine thymocyte has a reduced ratio of cholesterol (Chol) to phospholipids and a high amount of unsaturated phospholipids in comparison to the membrane of normal murine cells [12]. Both facts determine the fluidity of the lipid bilayer, which appears to be closely associated with the proliferative and metastatic ability of the cancer cells [13].

There is a close connection between the anti-cancer drug efficacy and the effect of the drug with the cell membrane. According to Tsuchiya et al., if the drug induces rigidity on the membrane, it can inhibit the growth of tumor cells [13]. Moreover, there is a drug threshold concentration below which the drug induces fluidity on the cell membrane. Then again, some anti-cancer drugs are more effective on tumor cells than expected from their membrane-rigidifying effects, in which case the interaction of the drug with DNA and/or membrane proteins needs to be considered. Accordingly, the molecular characteristics of the drug can modulate the interactions with the lipid bilayer and alter the mechanism of drug transport into the cell [14]. In the case of anticancer drugs, passive diffusion is the common transport across the plasma membrane into the tumor [15]. The degree of lipophilicity determines the ability of the anticancer drug to be incorporated into the lipid bilayer. Further, depending on the drug molecule, also electrostatic interactions with the lipid polar head should be considered.

Using Langmuir lipid monolayers as cell membrane models to study the effect of different drugs has the advantage that many parameters of interest are easily controlled: lipid composition (mechanical properties of the monolayer), subphase, temperature and lateral pressure [16]. Interactions can be assessed by solubilizing the drug in the subphase or by compressing the monolayers formed with mixed drug-lipids systems and can be studied by monitoring changes in the molecular area or surface pressure. In addition, lipid monolayers are very well-defined, stable and homogeneous bidimensional systems with planar geometry [5]. This classical technique provides valuable information at a molecular level. Under quasi-equilibrium conditions of the film compression, it is possible to quantify the molecular interactions by thermodynamic analysis of the compression isotherms [17]. Over the last decade, several studies on the interaction of anticancer drugs with cell membrane models by using Langmuir monolayers have been produced and reported. Matyszewska et al. have studied the interaction of doxorubicin and idarubicin with monolayers of zwitterions 1,2-dimyristoyl-sn-glycero-3-phosphochloline (DMPC) and negatively charged 1,2-dimyristoyl-sn-glycero-3phospho-L-serine (sodium salt) (DMPS) as well as a 7:3 mixture of the two lipids [14]. The effect of chitosan on cell membrane models made by ternary mixtures of dipalmitoylphosphatidylcholine (DPPC), sphingomyelin (Sph) and Chol has been reported by Pereira et al. [18]. The same research group has studied the role of Sph on the interactions of gemcitabine with cell membrane models made by a quaternary mixture (DPPC, DPPS, Sph and Chol) [4]. Studies on the interaction of Minerval with lipid binary and ternary monolayers have been carried out by Węder et al. [19]. Xu et al. studied the surface behavior of DPPC and Cur [20]. A study on the interaction of a potential anticancer drug with phospholipids in simple healthy (DPPC) and cancerous (DPPS) cell membrane models has been developed by Salis et al. [21]. Sandrino et al. studied the interaction with a potential anticancer drug with dipalmitoylphosphatidylglycerol (DPPG) and DPPC and monolayers [22]. The effect of anticancer drug edelfosine on Sph and Chol model membrane was investigated by Hac-Wydro et al. [2]. These authors also studied the effect of edelfosine with a healthy cell membrane model (Chol:DPPC = 0.67) and with a cancerous cell membrane model (Chol:POPC = 0.25) [1]. Karewicz et al. studied the interaction of Cur with egg yolk phosphatidylcholine (EYPC) and dihexadecyl phosphate (DHP) simple and mixed monolayers [23]. A first conclusion extracted from the literature revision is the lack of a common model membrane used for healthy or cancerous cell membranes. Herein, the healthy cell membrane has been modeled by a mixed monolayer of DPPC and Chol in a molar ratio Chol:DPPC = 0.67 at the air-water interface. The cancerous cell membrane model is composed of Sph and a lower proportion of Chol (Chol:Sph = 0.25). The choice has been based on Hac-Wydro et al. [1] and Inbar et al. [24] works. DPPC was replaced by Sph in tumor membranes since this unsaturated lipid forms less cohesive and less condensed films providing higher fluidity to the membrane.

Cur, a natural product with low intrinsic toxicity, was chosen as a hydrophobic compound. It is a yellow substance from the polyphenol's superfamily. It is the most abundant active component of turmeric or commonly called, Indian spice, which is derived from the dried rhizome of the *Curcuma longa* plant. Curcumin is a natural compound used in traditional Chinese and Indian medicine, demonstrating numerous properties such as antioxidant, anti-inflammatory, analgesic, antiseptic, antiviral, and anti-cancer [25,26]. Cur operates its anti-cancer effects through different mechanisms. It inhibits cancer cell growth and proliferation in vitro and in vivo. Cur can induce apoptosis and autophagy by up-regulating pro-apoptotic proteins. It has also been reported to inhibit angiogenesis and suppress metastasis and invasion. In addition, it has been reported that Cur enhances the therapeutic effects of radiotherapy [27]. In pancreatic cancer, Cur has shown in vitro cytotoxic effect in several cell lines, and in vivo, it has shown to inhibit tumor growth thanks to the inhibition of angiogenesis and oxidative stress, and the promotion of apoptosis [28,29]. Moreover, the combination with other drugs has reported synergistic effects [30,31]. Recently, Gowhari Shabgah et al. [32]. have emphasized that these anti-cancer effects are principally attributed to the regulation of several cellular signaling pathways, and moreover, Cur can affect to the expression and function of the tumor-suppressive and oncogenic long non-coding RNAs. Accordingly, Cur was added to both cell membrane models in various mole fractions (χ_{Cur}= 0; 0.3; 0.5; 0.7; 1.0) and its effectiveness in the anticancer treatments is determined by studying its effect on the thermodynamic stability of both membrane models and the compressibility of the monolayers. Moreover, Brewster Angle Microscopy (MicroBAM) and Atomic Force Microscopy (AFM) allow visualization of the different monolayers and interaction mechanisms. As a result, we provide evidence of the applicability of Langmuir monolayers as a valuable biotechnological tool to monitor the efficacy of cancer treatments in model lipid membranes.

2. Materials and methods

2.1. Film components and monolayer solutions

Membrane models were prepared using 2-dipalmitoyl-sn-glycero-3-phosphocholine (DPPC) purchased from Avanti Polar Lipids Inc® (product number 850355P), and cholesterol (Chol) and sphingomyelin (Sph) supplied by Sigma - Aldrich Inc® (C8667 and S-0756 respectively). Curcumin (Cur) from Sigma - Aldrich Inc® (C1386) was used as anti-cancer hydrophobic compound. Fig. 1 shows the chemical structure of all of them, the molecular structure of sphingomyelin presents a phosphocholine head-group, sphingosine, and fatty acid, while the molecular structure of DPPC consists of two C_{16} palmitic acid groups attached to a phosphocholine head-group. Lipids were stored at 4 ºC, Cur was stored at room temperature, and all components were used without further purification.

To prepare the spreading organic solutions, chloroform (HPLC grade, ≥99.5%) purchased from *Alfa Aesar* and methanol (HPLC grade, ≥99.9%) from *Scharlau* were used.

The subphase was a PBS buffer at pH 7.4 supplied by *Medicago*. Double distilled water (Millipore Milli-Q Reagent Water System) was utilized both for cleaning purposes and to prepare the buffer solutions.

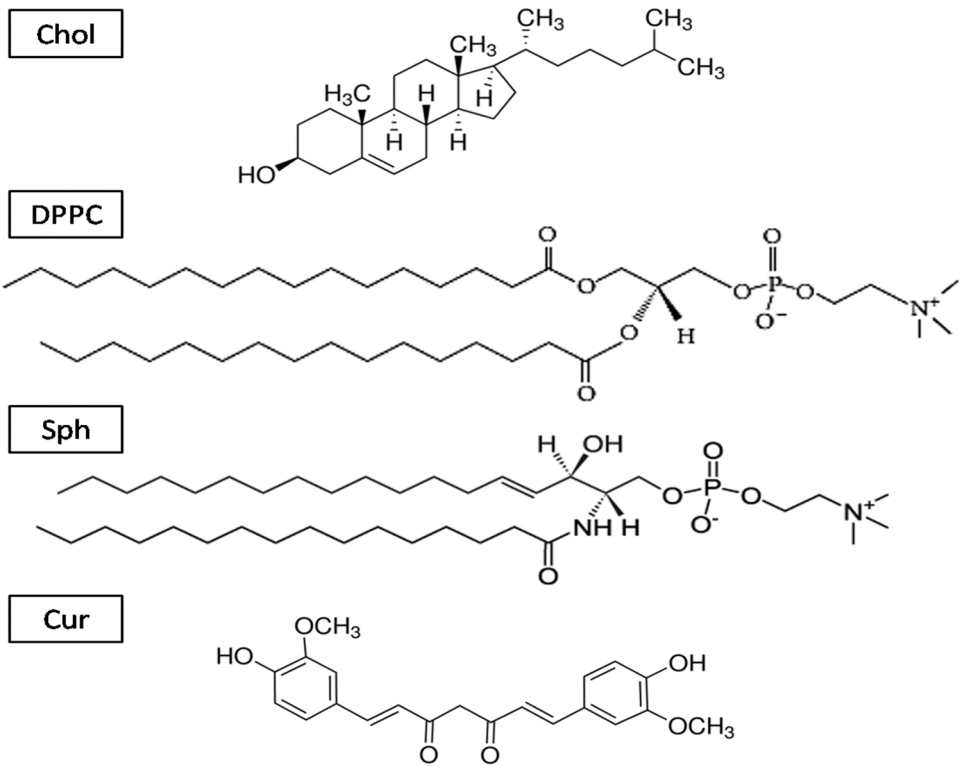

Fig. 1. Chemical structure of cholesterol, dipalmitoylphosphatidylcholine, sphingomyelin and curcumin molecules.

The conductivity of the water after the distilling process was always lower than 2 μS/cm and its pH was 6–6.5.

The solvent for solutions involving only DPPC and Chol was chloroform, whereas for solutions involving Sph and Cur was a methanol-chloroform mixture in a 1:4 ratio. Solutions were prepared in glass vials and stored at − 18 °C until used. The concentration of all spreading organic solutions was 0.5 mg mL^{-1}.

2.2. Langmuir monolayer formation and compression isotherms

The surface pressure-area (π-A) isotherms for lipid and mixed monolayers have been recorded using a KSV Minitrough from KSV Instruments, a commercial version of a Langmuir-film balance (total area = 237.75 cm^2) placed on an anti-vibrational table. The curcumin film has been recorded with a KN0032-KSV NIMA Langmuir-Blodgett Trough Top Small (total area = 98 cm^2). Surface pressure (π) was measured using a Wilhelmy plate made of filter paper connected to an electrobalance (accuracy of ± 4 μN). The surface was symmetrically compressed employing two moving barriers at a speed of 10 mm min^{-1} with an accuracy of 1%. The subphase temperature was fixed to 20 ± 1 ºC by a circulating water system connected to a thermostat (*FRIGITERM TFT-10*).

Prior to each measurement, all components of the though were meticulously cleaned with pure isopropanol and double distilled water until no impurities were detected in the buffer, and the electrobalance was calibrated. The absence of impurities was tested by compression of the buffer-air interface obtaining values of $\pi < 0.2$ mN m^{-1} at the maximum compression.

For lipid films and their mixture with low Cur proportions, a volume of 50 μL of solution (0.5 mg mL^{-1}) was spread, whereas for mixtures with a high amount of Cur or pure Cur films a volume of 60 or 80 μL (0.5 mg mL^{-1}) was used. The dissolutions were carefully spread on the buffer surface in the form of small drops with the help of a Hamilton® 700 series syringe (± 1.0 μL) and left for 10 min to allow evaporation of the solvent. The syringes employed in solution spreading were flushed with chloroform before and after each use to assure the absence of surface-active contaminants. To check the reproducibility of the π-A compression isotherms, each experiment was repeated at last twice.

2.3. MicroBAM and AFM imaging

MicroBAM images of the lipid films were taken using a Brewster Angle Microscopy using a KSV NIMA MicroBAM (Biolin Scientific, Gothenburg, Sweden) equipped with a 50 mW laser emitting p-polarized light of 659 nm. The MicroBAM is mounted on the Langmuir trough and images of each film were taken in situ every 3 s during the full compression process.

For AFM imaging, the monolayers were transferred onto freshly cleaved mica (Agar Scientific) by the Langmuir-Blodget (LB) technique. The mica support was immersed in the clean subphase before spreading the lipid monolayer and it was extracted vertically at 30 mN m^{-1} compression. The transfer rate was 5 mm min^{-1}. After drying at room temperature, the transferred monolayers were observed using an Atomic Force Microscope Nanoscope IV MultiMode in air (Digital Instruments, Santa Barbara, Ca, USA). Images were obtained in tapping mode with a monolithic silicon AFM probe with an aluminum reflective coating and a resonance frequency of 150 kHz. The topography data were sampled in a grid of 512 × 512 points. Imaging was carried out under ambient laboratory conditions. Each sample was imaged in at least two different areas obtaining similar patterns. AFM images were processed and analyzed using Gwyddion Open-Source software.

3. Results and discussion

3.1. Surface pressure - area (π-A) isotherms and compression modulus of lipid monolayers

Fig. 2A shows the π-A isotherms recorded for the individual lipids and mixed monolayers modeling the healthy and tumor cell membrane models. Fig. 2B shows the compression modulus of the monolayer, C^{-1},

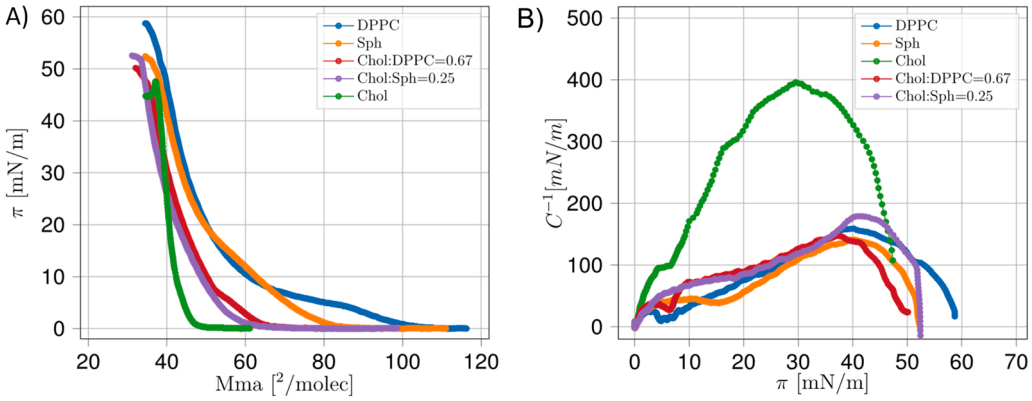

Fig. 2. (A) π versus Mma compression isotherms and (B) compression modulus C^{-1} versus π of pure DPPC (blue), Sph (orange), Chol (green), healthy cell model: Chol:DPPC = 0.67 (red) and cancerous cell model: Chol:Sph= 0.25 (purple). Monolayers were spread on PBS 7.4, 20 °C. Plotted values are mean values with standard deviations < 2%.

as a function of π-obtained for individual lipids, healthy and cancerous cell membrane models. C^{-1} values are calculated from the experimental isotherms plotted in Fig. 2A by using Eq. 2 [1].

$$C^{-1} = -\left[\frac{1}{A}\left(\frac{dA}{d\pi}\right)_T\right]^{-1} \quad (1)$$

where A is the area per molecule at a given π. This parameter is the inverse of the compressibility coefficient of the film, also known as in-plane elasticity [21].

The obtained results for individual lipids are consistent with literature data of these well-known lipids [4,33–35]. Results shown in Fig. 2A prove that Chol constitutes the most condensed monolayer, as the ***π***-A isotherm appears located at the lower mean molecular areas (Mma) [36]. Also, the maximum compression modulus, obtained at 30 mN m^{-1}, reaches around 400 mN/m, a value that falls within the range of the liquid-condensed (LC) phase [14]. The rest of the isotherms for pure lipids (DPPC and Sph) show a more extended conformation since their ***π***-A isotherms appear displaced to higher Mma (Fig. 2A). The ***π***-A isotherm obtained for DPPC displays a phase transition at around 7–8 mN m^{-1} (Fig. 2A), which is identified by a local minimum of C^{-1} at this ***π*** (Fig. 2B). The low value of C^{-1} (less than 100 mN m^{-1}) obtained within the whole compression 0–30 mN m^{-1} indicates that the DPPC monolayer stands in LE phase until 30 mN m^{-1}. Upon further compression, at around 40 mN m^{-1}, the C^{-1} reaches a maximum with a value slightly higher than 150 mN/m (Fig. 2B). This all agrees with previous works [36]. The ***π***-A isotherm obtained for Sph shows a phase transition at around 15 mN m^{-1}(Fig. 2A). Again, this phase transition is identified in Fig. 2B by a minimum in C^{-1} located at this same ***π***. The values of C^{-1} are slightly lower than those for DPPC at LE conformation. At 40 mN m^{-1} the value of C^{-1} reaches a maximum (just above 150 mN/m), meaning that the LC phase of Sph appears somewhat less compressible than DPPC in LC phase. These results again agree with literature data of Sph Langmuir monolayer [37].

Concerning the healthy cell model membrane (Chol:DPPC = 0.67) and cancerous (Chol:Sph = 0.25) also displayed in Fig. 2A. The ***π***-A isotherm corresponding to healthy cell model membrane shows an intermediate behavior compared with that shown by pure components, Chol and DPPC. The addition of Chol to DPPC decreases the average area per molecule and therefore, the isotherm of the mixed film appears between the isotherms of the pure components. Although the proportion of Chol in the mixture is high, the minimum in C^{-1} observed in Fig. 2B suggests that the isotherm still shows a phase transition around 15 mN/m. Despite the well-known condensation effect of Chol [38], the values of C^{-1} in all the compression range are similar to that of the DPPC monolayer.

Additionally, Fig. 2A presents the ***π***-A isotherm obtained for cancerous cell model membrane (Chol:Sph = 0.25). The cancerous cell membrane model film also presents a somewhat intermediate behavior compared to that of its pure components Chol and Sph. In this case, the condensing effect of Chol is less pronounced than that observed for healthy cell model membrane (Chol:DPPC = 0.67) since pure Sph monolayer is already more extended than DPPC monolayer and the proportion of Chol in tumor cell model membrane is lower than in the healthy one. Further, Fig. 2B shows that the isotherm only reaches a LC state [13] (given by a maximum compression modulus of 175 mN m^{-1}) at high compression rates (***π*** higher than 40 mN m^{-1}).

3.2. *Effect of Cur on π-A isotherms and compression modulus of healthy and cancerous cell membrane models*

Fig. 3 shows the effect of Cur in the ***π***-A isotherms and compression modulus recorded for Langmuir monolayers of the healthy cell membrane model, Chol:DPPC = 0.67, (Figs. 3A and 3B) and tumor cell membrane model, Chol:Sph = 0.25, (Figs. 3C and 3D), respectively.

The characteristic parameters from these isotherms are displayed in Table 1. It is important to underline that the impact of drug addition on membrane fluidity is directly related to the biological action of drugs44, therefrom the importance to analyze the compression modulus of the monolayers.

The ***π***-A isotherm obtained for pure Cur reveals the surface activity of this compound on PBS subphase, which lifts off at the Mma of 23.5 A^2/molecule (Figs. 3A and 3C). The ***π*** increases smoothly in a first compression regime that lasts until a ***π*** of around 39.6 mN m^{-1}. No experimental evidence of collapse has been observed. The values of the compression modulus remain under 55 mN/m, which are typical values for a LE phase [14]. The limiting molecular area value calculated from the isotherm of Cur film agrees with its molecular structure. According to the shape of the molecule, it seems to be horizontally oriented with all the polar groups (-OH, -OCH3) on both sides of the aromatic rings and two C═O groups anchored in the water. Different ***π***-A isotherms have been reported for Cur monolayer in the literature. Karewicz et al. [23] and more recently by Zembyla et al. [39] show a lower maximum ***π*** while Xu et al. [20] reach higher compression states. We hypothesize that the amphiphilic character is due to the presence of hydrophilic (-OH, OCH_3, C═O) and hydrophobic groups, as demonstrated in Fig. 3, S1, S2.

The effect of Cur on healthy and tumor membrane cell models can be now discussed by analyzing the curves presented in Fig. 3. The ***π***-A isotherms corresponding to the interaction of Cur with a healthy cell membrane model (Chol:DPPC = 0.67), added in different mole fractions, are represented in Fig. 3A. Increasing the concentration of drug yields to a gradual shift of the isotherms towards smaller areas to an extent that nearly follows the same proportion as the molar ratio of Cur in the

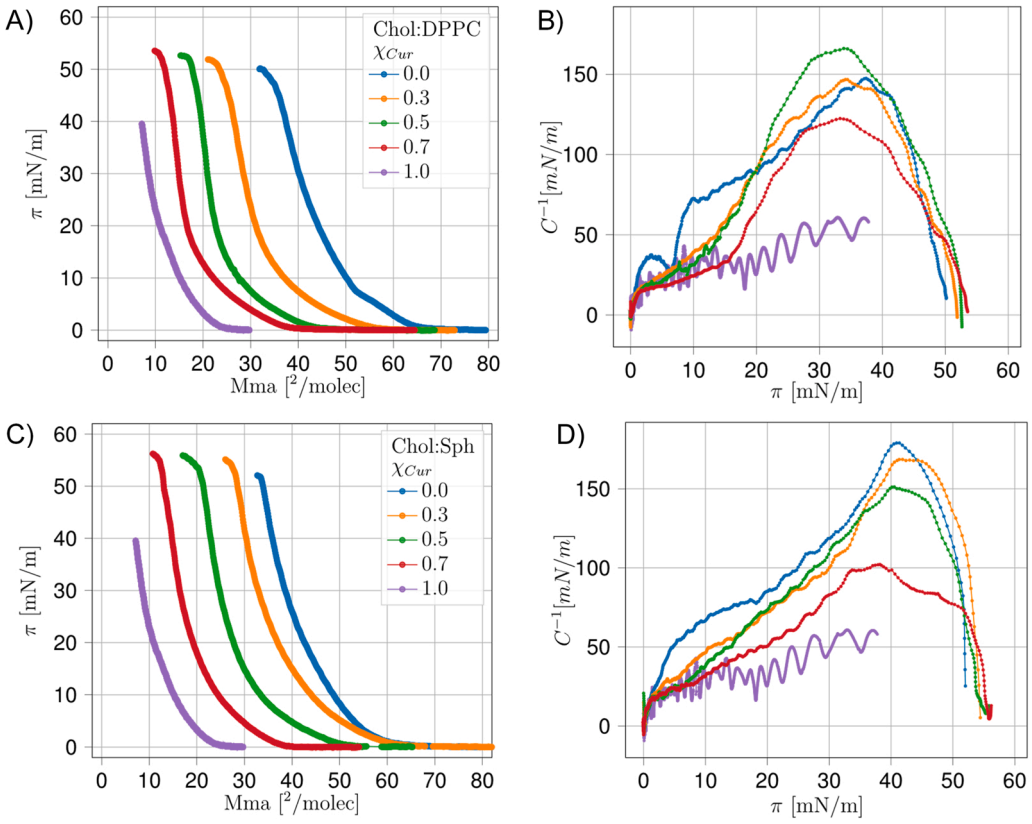

Fig. 3. π versus Mma isotherms and compression modulus C^1 versus π as the molar fraction of Cur (χ_{Cur}) increases in the monolayer for (A, B) healthy cell model membrane (Chol/DPPC = 0.67) and for (C,D) cancerous cell model membrane (Chol:Sph = 0.25). Monolayers were spread on PBS pH 7.4 at 20 °C. Plotted values are mean values with standard deviations < 2%.

Table 1
Limiting molecular area A_0, collapse pressure π_c and compression modulus C^{-1}_{cell} at cell membrane lateral pressure (30 mN/m) of DPPC/Chol/Cur and Sph/Chol/Cur monolayers at different Cur concentrations π_{Cur} as given in Fig. 3.

	DPPC/Chol/Cur			Sph/Chol/Cur		
χ_{Cur}	A_0 [Å²/ molec]	π_c [mN/ m]	C^{-1}_{cell} [mN/m]	A_0 [Å²/ molec]	π_c [mN/ m]	C^{-1}_{cell} [mN/m]
0.0	48.30	50.15	126.60	44.39	53.01	118.66
0.3	34.25	51.90	136.42	38.00	55.87	100.11
0.5	24.73	52.51	161.06	29.08	56.23	108.63
0.7	18.58	53.58	118.38	20.95	56.30	82.98
1.0	13.44	–	51.24	13.44	–	51.24

mixture. This result is quantified by the value of the limiting molecular area, A_0, reported in Table 1: A_0 values decrease with the proportion of Cur in the film. Moreover, the mixed (Chol:DPPC = 0.67) monolayer slightly resembles the steeper curve obtained for the Cur monolayer as the amount of Cur increases in the mixture. Even the phase transition for Chol:DPPC = 0.67 disappears in the presence of Cur. Therefore, the addition of small proportions of Cur, lightly condenses the monolayer corresponding to the healthy model. Similar behavior was found by Xu et al. [20] studying the interaction of Cur with DPPC films. However, the compression modulus in Fig. 3B does not evidence a marked change in the Chol:DPPC = 0.67 monolayer fluidity. Only when the mole fraction of Cur is 0.5, the maximum value of C^{-1} of the healthy model slightly increases. Karewicz et al. found a small increase of the C^{-1} maximum value when Cur was added to an EYPC monolayer. Therein, a condensing effect of Cur on the EYPC film was hypothesized [23]. In contrast, the small reduction of C^{-1} at a higher mole fraction of Cur (0.7) shown in Fig. 3C illustrates a slight fluidizing effect on the healthy cell membrane induced by Cur. Interestingly, at a π value of 30 mN/m, the values of compression modulus displayed in Table 1 increase with the amount of Cur until a mole fraction of 0.5 and decrease at a 0.7 mol fraction of Cur. Anyhow, all C^{-1} values are higher than 100 at π above 25 mN m^{-1}, indicative of a LC state of the monolayer in all cases. It should also be noted that the π_c value slightly increases with the proportion of Cur in the monolayer (Table 1).

Fig. 3C presents the π-A compression isotherms registered for the cancerous cell membrane model (Cho:Sph = 0.25) with different mole fractions of Cur in the monolayers. Fig. 3D shows the C^{-1} values versus π. The addition of Cur to the tumor cell membrane model film also displaces the π-A isotherms towards smaller molecular areas. This apparent condensation effect of Cur is accompanied by a reduction of the compression modulus with the proportion of Cur in the lipid mixture (Fig. 3D). At the higher proportion of Cur, the obtained value of C^{-1}_{cell} just below 100 mN m^{-1} indicates that the film even reaches the LE phase. Similar behavior was also reported in systems of DPPC and DPPS monolayers with PMN1 as drug candidate [21]. Salis et al. argued that a reduction of maximum C^{-1} indicates a more flexible monolayer in terms of molecular rearrangements when it responds to the compression. Matyszewska et al. also observed a reduced C^{-1} maximum value when doxorubicin or idarubicin (anti-cancer drugs) were added to DMPC or DMPS monolayers as cell membrane models [14]. This behavior was interpreted as fluidization of the phospholipid chains induced by drug-lipid interactions. Materon et al. also observed a decrease of the compressibility modulus when gemcitabine (GEM) –an anti-cancer drug- was added into a DPPC:DPPS:Chol membrane model monolayer, inducing an increased fluidity in the Langmuir films44. The same behavior was observed by Węder et al. [19] when an anticancer drug, 2-hydroxyoleic acid (2OHOA) was mixed with Chol, Sph or POPC lipids in a Langmuir monolayer. The compression modulus decreases in all cases making the films more fluid. Sandrino et al. studied the correlation

of an antitumor of ruthenium complex with the elasticity of cell membrane models forming by DPPC or DPPG Langmuir films. In both cases, the C^{-1} maximum value decreases with the proportion of the drug into the film and again, the authors indicated that this is due to the fluidization of the monolayers [22].

Comparing the effect of Cur on both healthy and tumor cell membrane models, the more significant result is that Cur makes more fluid the cancerous cell membrane model than its healthy counterpart. And thusly, the maximum values of C^{-1} appear at higher compression states for the cancerous cell model membrane. Namely, the maximum is located at $\pi \sim 40$ mN/m for (Chol:Sph = 0.25) monolayers and at $\pi \sim 32$ mN/m for the (Chol:DPPC = 0.67) monolayers. Moreover, according to Table 1, at the lateral pressure of the membranes (30 mN/m) and for different proportions of Cur, the values of C^{-1} are higher than 100 mN m^{-1} for the healthy and lower than 100 mN/m for the tumor cell membrane model.

3.3. Interaction parameters of Cur with healthy and cancerous cell membrane models: excess areas (A_{exc}) and excess free energy of mixing (ΔG_{ex})

To better understand the effect of Cur on cell membrane models and to quantify the interactions between both, the excess area (A_{exc}) and excess free energy (ΔG_{exc}) as a function of the molar fraction of Cur for some compression states have been calculated according to the following equations [1,4].

$$A_{exc} = A_{123} - A_{id} = A_{123} - A_{12}(\chi_1 + \chi_2)A_3\chi_3 \quad (2)$$

$$\Delta G_{exc} = N\int_0^{\pi}(A_{123} - A_{12}(\chi_1 + \chi_2) - A_3\chi_3)d\pi \quad (3)$$

Where label 1 refers to DPPC or Sph for each model, 2 to Chol, and 3 to Cur. A_{id} represents the ideal area per molecule obtained from the additivity rule. To obtain the ΔG_{exc} values, the integral has been calculated for π between 0 and 30 mN m^{-1}.

Fig. 4 shows the excess molecular area and the excess free energy versus the mole fraction of Cur for healthy and cancerous membrane models calculated for different compression states of the monolayer, i.e., different π. Concretely, the effect of Cur on the Chol:DPPC = 0.67 monolayer is shown in Figs. 4A and 4C, and the effect of Cur on Chol:Sph = 0.25 monolayer is shown in Fig. 4C and D.

Regarding the effect of Cur on the excess molecular area obtained for healthy cell membrane model (Chol:DPPC = 0.67), Fig. 4A shows negative deviations from ideal behavior, mainly at low compression states of the monolayer ($\pi = 5$ and 15 mN m^{-1}), being especially noticeable at a mole fraction of Cur of 0.5. Similarly, Fig. 4C also shows negative values of ΔG_{exc} with a maximum located at the same mole fraction of Cur. This behavior indicates that the mixture of Cur with the healthy cell membrane model (Chol:DPPC = 0.67) is thermodynamically favored, possibly due to attractive interactions between Cur and the lipids Chol and DPPC.

Regarding the effect of Cur on the excess molecular area obtained for the cancerous cell membrane model (Chol:Sph = 0.25), Fig. 4B shows positive deviations from the additivity rule for all compression states and mole fraction of Cur, except for $\pi = 5$ mN/m and mole fraction χ_{Cur}

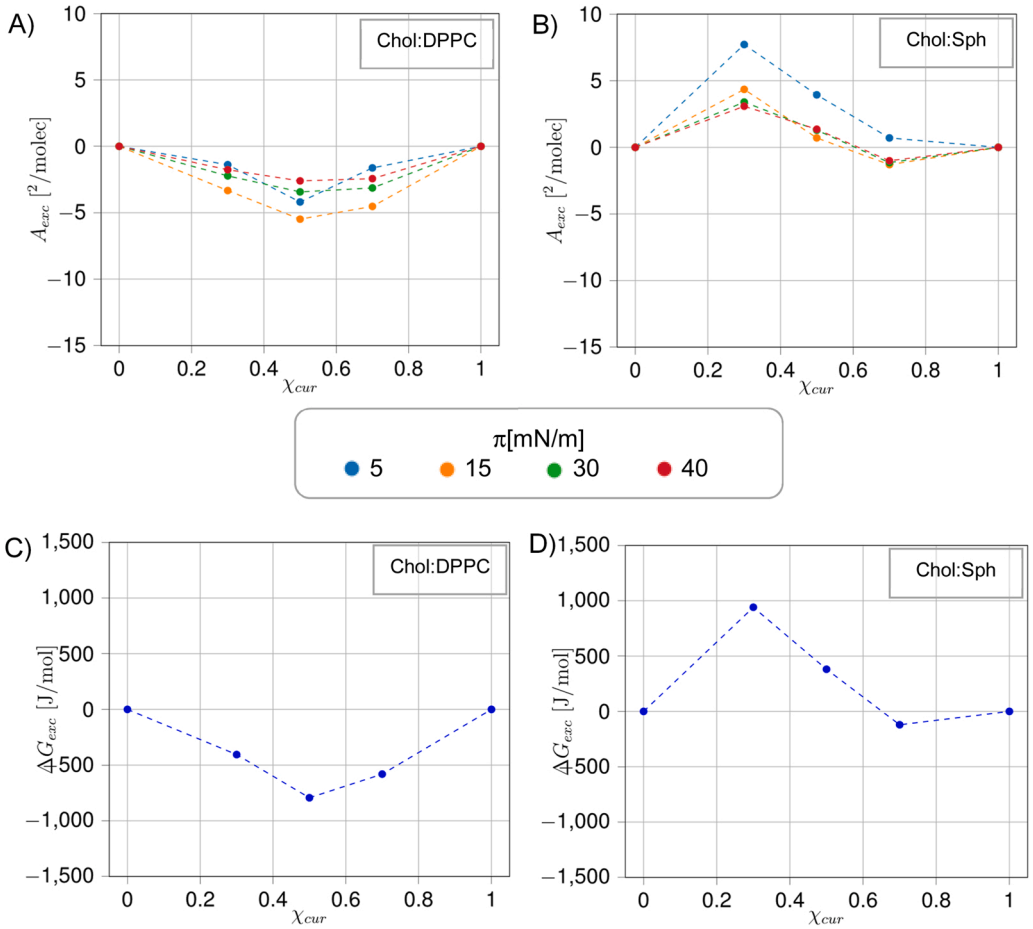

Fig. 4. Excess molecular area, A_{exc}, and excess free energy of mixing, ΔG_{exc}, calculated for Chol:DPPC = 0.67/Cur (A and C) and Chol:Sph = 0.25/Cur (B and D) represented versus the mole fraction of Cur (χ_{Cur}) at compression states: $\pi = 5$ mN m^{-1} (blue), $\pi = 15$ mN m^{-1} (orange), $\pi = 30$ mN m^{-1} (green), $\pi = 40$ mN m^{-1} (red). Plotted values are mean values with standard deviations < 5%.

= 0.7, where it shows a slightly negative deviation from ideal behavior. Positive deviations from ideal behavior are indicative of the existence of repulsive interactions between the cancerous cell membrane model (Chol:Sph = 0.25) and Cur. Specifically, the values of ΔG_{exc} plotted in Fig. 4D confirm that, at low proportions, Cur destabilizes the tumor cell membrane model. These findings obtained for model systems importantly correlate with results obtained for isolated lipids from breast cancer cells, showing different degrees and patterns of interaction of doxorubicin with resistant cell membrane lipids [40].

Results from Fig. 4 suggest the existence of interactions between Cur and healthy and cancerous cell membrane models whose impact depends not only on the proportion of drug but also largely on the compression state of the monolayer as given by the π. The intermolecular distance of lipids in the monolayer clearly determines to a large extent the degree and pattern of interaction with drugs. Moreover, the composition of the monolayer and the proportion of Chol used in the lipid membrane model determines the fluidity of the monolayers, also affecting critically and modulating the interactions with the drug.

3.4. MicroBAM and AFM imaging of Cur with healthy and cancerous cell membrane models

Fig. 5 shows a series of representative MicroBAM images of healthy and cancerous cell membrane models obtained before and after the addition of different mole fractions of Cur in the monolayer. All images are taken at π= 30 mN m^{-1}, corresponding to the compression state of cell membranes. In the absence of Cur (Figs. 5A and 5E) MicroBAM images show homogeneous bright coverage corresponding to a film in LC state formed in both cases. Indeed, images of the monolayer composed of Shp:Chol = 0.25 (tumor cell, Fig. 5E) appear slightly more homogeneous than those obtained for monolayers composed of DPPC: Chol = 0.65 (healthy cell, Fig. 5A). This is possibly due to the higher concentration of Chol used in the healthy cell membrane model which produces small rafts of condensed Chol aggregates (brighter circular domains in Figs. 5A and 5E).

The addition of Cur to the system induces domain formation in monolayers formed by both healthy (Figs. 5B, 5C and 5D) and cancerous (Figs. 5F, 5G and 5H) cell membrane models. However, this effect is less notorious in monolayers composed of Chol: DPPC = 0.67 (healthy cells), since a large amount of film remains in LC state in presence of Cur. In this model, it is also observable the formation of areas with a filament-like brighter shape, that could be condensed regions of Chol rafts as the proportion of Cur increases in the system. On the contrary, in the monolayer composed of Chol:Sph = 0.25 (tumor cells) the phase separation induced by Cur seems to be more notorious (Figs. 5F, 5G and 5H). The homogeneous LC state of the monolayer composed of Chol:Sph = 0.25 (Fig. 5E) starts showing some darker regions corresponding to LE state upon addition of Cur in the system. As the proportion of Cur is increased, these regions at LE state become more evident and even become equal in area to the regions in LC state. This phenomenon confirms the fluidizing effect that Cur has in the cancerous cell membrane model and may prove that the cohesion in monolayers formed by Chol:Sph = 0.25 decreases with the addition of Cur, according to the positive o zero values of ΔG_{exc} shown in Fig. 4D.

With the aim to check the stability of the Cur films different MicroBAM images have been recorded at different surface pressure values. These results are shown in Fig. S2, confirming that Cur forms stable films at the interface air-PBS.

A more detailed analysis of the changes Cur induces in the morphology of lipid monolayers is performed via AFM imaging of LB films. Fig. 6 shows a series of representative AFM micrographs of healthy and cancerous cell membrane models obtained before and after the addition of different mole fractions of Cur in the monolayer, including a micrograph of the pure Cur film. Images were taken on LB films transferred to mica at π = 30 mN m^{-1}, as in Fig. 5. AFM images of monolayers composed of Chol:DPPC = 0.67 (healthy cell membrane model) provide a homogeneous micrograph in the absence of Cur (Fig. 6A). A rough background appears spotted with a few spherical structures, all of them with similar shape and size (of around 4.3 nm in width and 1.8–2.2 nm in height). When zooming in the image, it can be observed that these spheres seem to be embedded into the film since they are surrounded by a lower area (Fig. 7A). This morphology has been reported by other authors in Chol:DPPC mixed films [41]. On the contrary, AFM images of monolayers composed of Chol:Sph = 0.25 (cancerous cell membrane model) appear more heterogeneous and exhibit superposed circular areas of different widths lying between 70 nm and 90 nm (Fig. 6E). When zooming into the image, it can be observed that they enclose small clusters of 2.3–2.8 nm in height (Fig. 7B). Fig. BI shows that Cur forms a highly homogeneous film of ~1.25 nm in height that almost completely covers the full substrate, indicating that Cur can form Langmuir films and do not aggregate in lenses.

When Cur was added into the system, the morphology of both monolayers (healthy and tumor cell membrane models) changes drastically, indicating again that Cur interacts with both types of films. Filament-like domains with terraces at different heights build by aggregates of globular structures appear on the base film, indicating the

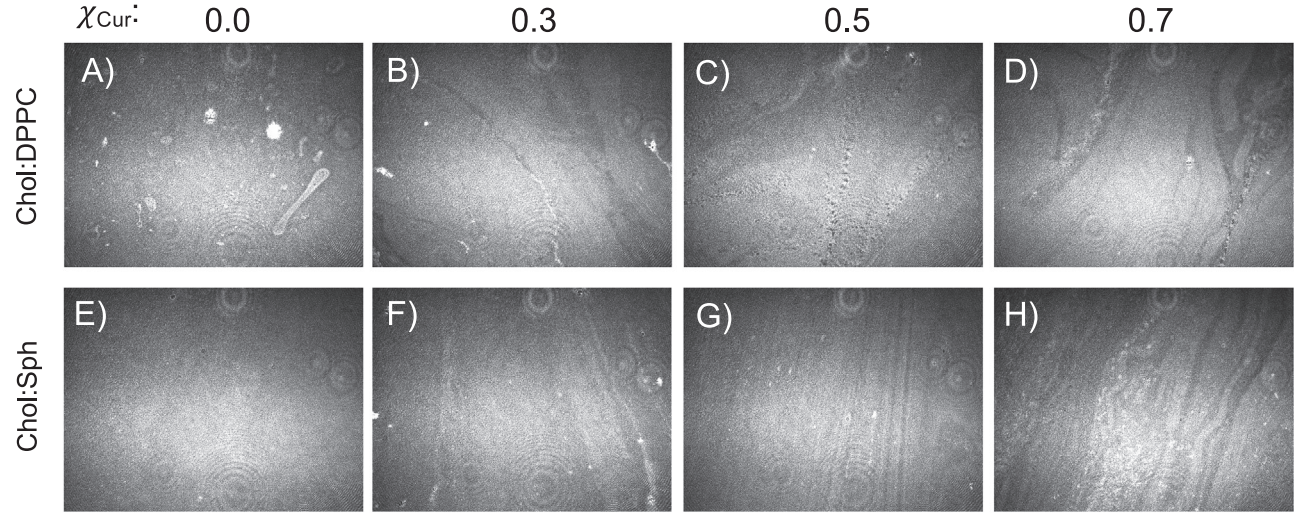

Fig. 5. MicroBAM images of Chol:DPPC (top) and Chol:Sph (bottom) films before (A and E) and after the addition of different Cur concentrations: χ_{Cur} = 0.3 (B and F), 0.5 (C and G) and 0.7 (D and H). The field of view is 3584 × 2688 μm. All images were taken at π = 30 mN m-1, PBS buffer, pH 7.4 and 20 ºC.

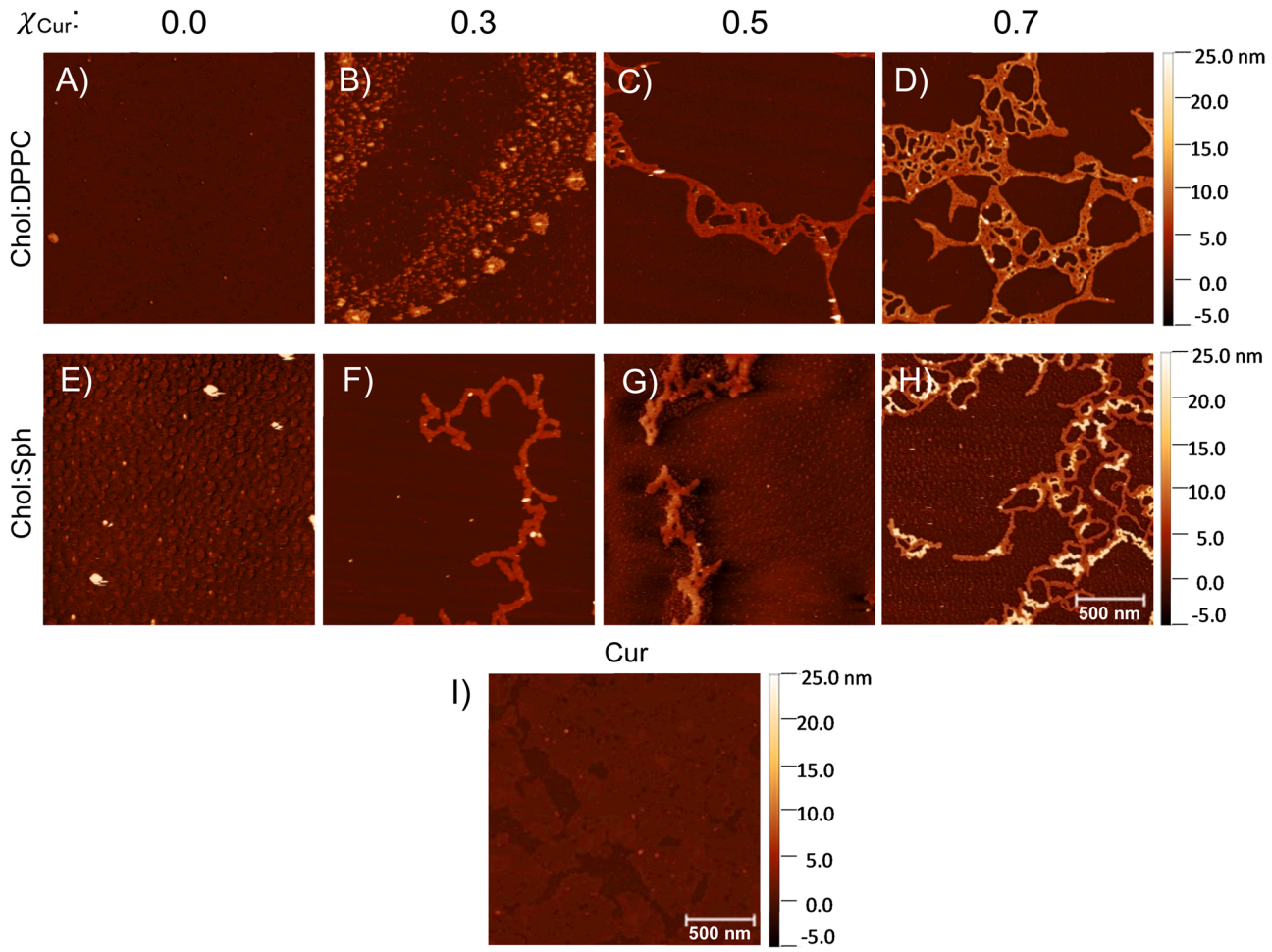

Fig. 6. AFM images of the effect of Cur on the morphology of Chol:DPPC (top) and Chol:Sph (bottom) monolayers, and I) pure Cur monolayer. The images correspond to films of a one-monolayer thick at different Cur mole fractions: 0.0 (A and E), 0.3 (B and F), 0.5 (C and G) and 0.7 (D and H). LB films were transferred at 30 mN/m to a mica substrate and were taken at ambient conditions. The field of view is 2 μm × 2 μm.

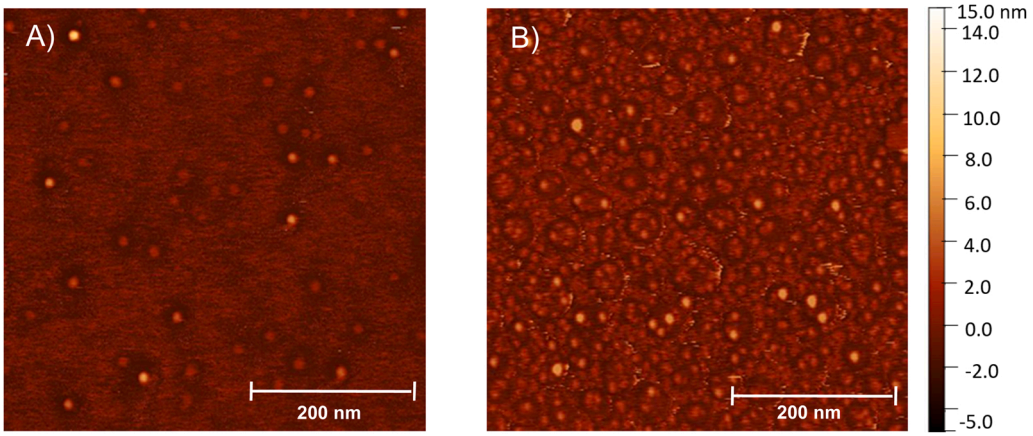

Fig. 7. Zoom in AFM images of (A) Chol:DPPC and (B) Chol:Sph monolayers. LB films were transferred at 30 mN/m to a mica substrate and were taken at ambient conditions. The field of view is 0.5 μm × 0.5 μm.

presence of phase separate elements. Additionally, they grow and become more frequent as the proportion of Cur increases in the monolayer. This happens for healthy and cancerous cell membrane models, however, there are some peculiarities in each case.

Figs. 6B, 6C and 6D correspond to a monolayer composed of Chol:DPPC = 0.67 (healthy cell model). Bands of irregular clusters first appear at $\chi_{Cur} = 0.3$. These clusters are circular when they are small and seem to merge as the size of the cluster grows to larger irregular structures with two flats levels at ~3 nm and ~8.22 nm, with embedded circular structures of 15.6 nm in height (Fig. 6B). When the χ_{Cur} was increased to 0.5 (Fig. 6C), the clusters merge to form wide filaments with interconnected areas and which are homogeneous in height. Only one

terrace of 4.7 nm high is distinguished, which can get to up to 270 nm in width. At $\chi_{Cur} = 0.7$, more filaments appear, and the plateau grows to ~6.8 nm in height. Circular bright spots become more frequent and show two different heights at ~11.8 nm and ~30 nm (Fig. 6D). The spherical structures on the filaments seem to be aggregates of Cur.

Figs. 6F, 6G and 6H correspond to a monolayer composed of Chol:Sph = 0.25 (tumor cell model). Narrow filaments appear even at low Cur proportion (Fig. 6F). These filaments are similar to the ones appearing in monolayers of Chol:DPPC = 0.67 (Fig. 6B) but thinner, higher and with lobulated borders. At $\chi_{Cur} = 0.3$ they only exhibit one terrace of ~5.20 nm in height which reaches less than 70 nm in width (Fig. 6F). At $\chi_{Cur} = 0.5$ the terrace at 5 nm seems to break into small clusters and another terrace appears at around ~13.5 nm (Fig. 6G). When Cur increases to 0.7, the shorter terrace grows to ~7 nm without modifying the one at 13.5 nm, and rows of ~21.4 nm high bright dots appear (Fig. 6H). In all images, except the one at $\chi_{Cur} = 0.3$, the background appears similarly dotted as in the image in the absence of Cur (Fig. 6E). This could indicate that at $\chi_{Cur} = 0.3$, the interaction with the monolayer composed of Chol:Sph = 0.25 is altered. It is noticeable that this result coincides with the maximum positive values of ΔA_{exc} and ΔG_{exc} observed in Fig. 4 B and 4D, respectively.

It is expected that films formed by tumor cell membrane models are lower in height than healthy ones, given that the latter is more condensed due to the higher amount of Chol. The relative heights of the structures observed here are higher in Chol:Sph = 0.25 than in Chol:DPPC = 0.67 monolayers. This fact could indicate that Cur disrupts more the tumor cell membrane model than the healthy one. This result would be again in agreement with the lower ΔG_{exc} reported previously for the healthy model.

4. Conclusions

Langmuir monolayers reveal as a useful biotechnological platform to test the potential of novel anti-cancer compounds. Modeling healthy and tumor cell membranes with lipid monolayers has a broad advantage due to the ease of controlling the lipid composition, and hence the fluidity of the membrane, as well as tuning the lateral pressure to match that of the biological membranes. Further, the analysis of Langmuir monolayers provides information on the degree and pattern of surface interactions at a molecular level. From the π-A isotherms registered by compression of the surface area it is possible to obtain thermodynamic properties and quantify the molecular interactions in the monolayer. In this work, the interaction of curcumin with monolayers composed of Chol:DPPC = 0.67 and Chol:Sph = 0.25, accounting for healthy cell membrane model and cancerous cell model membrane, respectively, have been measured, imaged and analyzed. The most remarkable result is the evidence of strong destabilization of the tumor cell membrane model by Cur, which is not evidenced in the healthy cell membrane model. The presence of Cur in the healthy cell membrane model improves its cohesion. Conversely, the presence of Cur in cancerous cell model membrane seems to impart repulsive forces in the monolayer causing thermodynamic destabilization and fluidizing. Results presented here indicate that Cur disrupts to a larger extent the tumor cell membrane model (composed of a lower proportion of cholesterol and an unsaturated lipid) than the healthy cell membrane model (with a higher concentration of cholesterol and a saturated lipid). Findings from this study on model membranes provide a better understanding of the action mechanisms of anti-cancer compound on cell membranes. This study might be helpful to improve transport of bioactives through the lipid bilayer in cell membranes which can improve current anti-cancer treatments.

CRediT authorship contribution statement

María Pedrosa: Methodology, Validation, Formal analysis, Investigation, Visualisation, Writing - Original Draft. **Julia Maldonado Valderrama**: Conceptualization, Writing - Review & Editing, Supervision. **María José Gálvez-Ruiz**: Conceptualization, Writing - Review & Editing, Supervision, Project administration, Funding acquisition.

Declaration of Competing Interest

The authors declare that they have no known competing financial interests or personal relationships that could have appeared to influence the work reported in this paper.

Acknowledgment

This work has been supported by project RTI2018-101309-B-C21 funded by MCIN/AEI/10.13039/501100011033/FEDER. María Pedrosa Bustos thanks the FPU19/02045 fellowship funded by MCIN/AEI/10.13039/501100011033 and FSE. This work has been done in the framework of the doctoral of AAG in the Doctoral Programme in Physics and Space Sciences (B09/56/1) of the University of Granada. JMV acknowledges support from project PID2020-116615RA-I00 funded by MCIN/ AEI /10.13039/501100011033. This work was also partially supported by the Biocolloid and Fluid Physics Group (ref. PAI-FQM115) of the University of Granada (Spain). Funding for open access charge: Universidad de Granada / CBUA.

Appendix A. Supporting information

Supplementary data associated with this article can be found in the online version at doi:10.1016/j.colsurfb.2022.112636.

References

[1] K. Hac-Wydro, P. Dynarowicz-Łatka, Effect of edelfosine on tumor and normal cells model membranes-A comparative study, Colloids Surf. B Biointerfaces 76 (2010) 366–369.
[2] K. Hac-Wydro, P. Dynarowicz-Łatka, P. Wydro, K. Bak, Edelfosine disturbs the sphingomyelin-cholesterol model membrane system in a cholesterol-dependent way - The Langmuir monolayer study, Colloids Surf. B Biointerfaces 88 (2011) 635–640.
[3] T.M. Nobre, et al., Interactions of bioactive molecules & nanomaterials with Langmuir monolayers as cell membrane models, Thin Solid Films 593 (2015) 158–188.
[4] E.M. Materon, et al., Role of sphingomyelin on the interaction of the anticancer drug gemcitabine hydrochloride with cell membrane models, Colloids Surf. B Biointerfaces 196 (2020).
[5] C. Peetla, A. Stine, V. Labhasetwar, Biophysical interactions with model lipid membranes: applications in drug discovery and drug delivery, Mol. Pharm. 6 (2009) 1264–1276.
[6] A.I. Bunea, S. Harloff-Helleberg, R. Taboryski, H.M. Nielsen, Membrane interactions in drug delivery: model cell membranes and orthogonal techniques, Adv. Colloid Interface Sci. 281 (2020).
[7] D. Marsh, Lateral pressure in membranes, Biochim. Biophys. Acta vol. 1286 (1996).
[8] Brockman, H. Lipid monolayers: why use half a membrane to characterize protein-membrane interactions?
[9] J.J. Giner-Casares, G. Brezesinski, H. Möhwald, Langmuir monolayers as unique physical models, Curr. Opin. Colloid Interface Sci. 19 (2014) 176–182.
[10] V.How Rosilio, Can artificial lipid models mimic the complexity of molecule–membrane interactions? Adv. Biomembr. Lipid Self-Assem. 27 (2018) 107–146.
[11] Y. Andoh, S. Okazaki, R. Ueoka, Molecular dynamics study of lipid bilayers modeling the plasma membranes of normal murine thymocytes and leukemic GRSL cells, Biochim. Biophys. Acta - Biomembr. 1259–1270 (1828) 2013.
[12] W.J. van Blitterswijk, G. de Veer, J.H. Krol, P. Emmelot, Comparative lipid analysis of purified plasma membranes and shed extracellular membrane vesicles from normal murine thymocytes and leukemic GRSL cells, BBA - Biomembr. 688 (1982) 495–504.
[13] H. Tsuchiya, et al., Membrane-rigidifying effects of anti-cancer dietary factors, BioFactors 16 (2002).
[14] D. Matyszewska, E. Nazaruk, R.A. Campbell, Interactions of anticancer drugs doxorubicin and idarubicin with lipid monolayers: new insight into the composition, structure and morphology, J. Colloid Interface Sci. 581 (2021) 403–416.
[15] H. Cortés-Funes, C. Coronado, Role of anthracyclines in the era of targeted therapy, Cardiovasc. Toxicol. 7 (2007) 56–60.
[16] G. Brezesinski, H. Möhwald, Langmuir monolayers to study interactions at model membrane surfaces, Adv. Colloid Interface Sci. 100–102 (2003) 563–584.
[17] M.J. Gálvez-Ruiz, Different approaches to study protein films at air/water interface, Adv. Colloid Interface Sci. 247 (2017) 533–542.

[18] A.R. Pereira, et al., Enhanced chitosan effects on cell membrane models made with lipid raft monolayers, Colloids Surf. B Biointerfaces 193 (2020).
[19] K. Węder, M. Mach, K. Hąc-Wydro, P. Wydro, Studies on the interactions of anticancer drug - Minerval - with membrane lipids in binary and ternary Langmuir monolayers, Biochim. Biophys. Acta - Biomembr. 2329–2336 (1860) 2018.
[20] G. Xu, C. Hao, L. Zhang, R. Sun, Investigation of surface behavior of DPPC and curcumin in langmuir monolayers at the air-water interface, Scanning 2017 (2017).
[21] L.F.G. Salis, et al., Interaction of 3′,4′,6′-trimyristoyl-uridine derivative as potential anticancer drug with phospholipids of tumorigenic and non-tumorigenic cells, Appl. Surf. Sci. 426 (2017) 77–86.
[22] B. Sandrino, et al., Correlation of [RuCl3(dppb)(VPy)] cytotoxicity with its effects on the cell membranes: an investigation using langmuir monolayers as membrane models, J. Phys. Chem. B 118 (2014) 10653–10661.
[23] A. Karewicz, et al., Interaction of curcumin with lipid monolayers and liposomal bilayers, Colloids Surf. B Biointerfaces 88 (2011) 231–239.
[24] M. Inbar, et al., Fluidity difference of membrane lipids in human normal and leukemic lymphocytes as controlled by serum components, Cancer Res. 37 (1977) 3037–3041.
[25] F. Galisteo-González, et al., Albumin-covered lipid nanocapsules exhibit enhanced uptake performance by breast-tumor cells, Colloids Surf. B Biointerfaces 165 (2018) 103–110.
[26] A. Aguilera-Garrido, T. del Castillo-Santaella, F. Galisteo-González, M. José Gálvez-Ruiz, J. Maldonado-Valderrama, Investigating the role of hyaluronic acid in improving curcumin bioaccessibility from nanoemulsions, Food Chem. 351 (2021).
[27] X.Y. Xu, et al., Bioactivity, health benefits, and related molecular mechanisms of curcumin: current progress, challenges, and perspectives, Nutrients 10 (2018).
[28] S. Bimonte, et al., Curcumin anticancer studies in pancreatic cancer, Nutrients 8 (2016) 1–12.
[29] K. Schwarz, S. Dobiasch, L. Nguyen, D. Schilling, S.E. Combs, Modification of radiosensitivity by Curcumin in human pancreatic cancer cell lines, Sci. Rep. 10 (2020) 1–10.
[30] K. Yoshida, S. Toden, P. Ravindranathan, H. Han, A. Goel, Curcumin sensitizes pancreatic cancer cells to gemcitabine by attenuating PRC2 subunit EZH2, and the lncRNA PVT1 expression, Carcinogenesis 38 (2017) 1036–1046.
[31] M. Kanai, et al., A phase i study investigating the safety and pharmacokinetics of highly bioavailable curcumin (Theracurmin®) in cancer patients, Cancer Chemother. Pharmacol. 71 (2013) 1521–1530.
[32] A. Gowhari Shabgah, et al., Curcumin and cancer; are long non-coding RNAs missing link? Prog. Biophys. Mol. Biol. 164 (2021) 63–71.
[33] M.J. Gálvez Ruiz, M.A. Cabrerizo Vilchez, A study of the miscibility of bile components in mixed monolayers at the air-liquid interface I. Cholesterol, lecithin, and lithocholic acid, Colloid Polym. Sci. 269 (1991) 77–84.
[34] A. Sakai, et al., The lipid composition affects Trastuzumab adsorption at monolayers at the air-water interface, Chem. Phys. Lipids 227 (2020), 104875.
[35] A.R. Pereira, F.M. Shimizu, O.N. Oliveira, Cholesterol modulates the interaction between paclitaxel and Langmuir monolayers simulating cell membranes, Colloids Surf. B Biointerfaces 205 (2021), 111889.
[36] A. Martín-Molina, T. del Castillo-Santaella, Y. Yang, J. Maldonado-Valderrama, Condensation of model lipid films by cholesterol: specific ion effects, Coatings 9 (2019).
[37] X.M. Li, J.M. Smaby, M.M. Momsen, H.L. Brockman, R.E. Brown, Sphingomyelin interfacial behavior: the impact of changing acyl chain composition, Biophys. J. 78 (2000) 1921–1931.
[38] Z. Al-Rekabi, S. Contera, Multifrequency AFM reveals lipid membrane mechanical properties and the effect of cholesterol in modulating viscoelasticity, Proc. Natl. Acad. Sci. USA 115 (2018) 2658–2663.
[39] M. Zembyla, A. Lazidis, B.S. Murray, A. Sarkar, Water-in-oil pickering emulsions stabilized by synergistic particle-particle interactions, Langmuir 35 (2019).
[40] C. Peetla, et al., Drug resistance in breast cancer cells: Biophysical characterization of and doxorubicin interactions with membrane lipids, Mol. Pharm. 7 (2010) 2334–2348.
[41] Rincon, S. R. Formation and Characterization of Model Cell Membranes and Their Interaction With Magnetic. (2015).